2.4 IRRADIATION-DAMAGE BEHAVIOR IN ADVANCED STEELS — C. M. Parish, Y. Katoh, M. E. Bannister, K. A. Unocic, L. Tan, B.-K. Kim, D. T. Hoelzer (Oak Ridge National Laboratory), and S. J. Zinkle (University of Tennessee)

OBJECTIVE

Determine the helium mitigation response of candidate steels (NFA, CNA, ODS-FeCrAl) and compare relative to each other.

SUMMARY

Four iron-based alloys were investigated: a 9Cr NFA "9YWTV" containing Y-Ti-oxides, a 9Cr CNA containing TaC precipitates, and two Fe-12Cr-5Al ODS alloys containing mixed populations of Y-Al-oxides, Y-Zr-oxides and Y-Hf-oxides. In a D-T burning plasma environment, the 14 MeV neutrons produce copious helium transmutation and the materials ability to mitigate helium effects must be characterized for future fusion materials selection and development. Here, sequential He and Fe ion irradiation is combined with advanced post-irradiation characterization to compare the four materials' helium mitigation.

PROGRESS AND STATUS

Introduction

As a screening experiment to begin understanding helium mitigation effects, 650°C sequential irradiations were performed at the ORNL MIRF facility; simultaneous dual-beam irradiations are presently underway at the Kyoto University DuET facility. 9YWTV NFA (nanostructured ferritic alloy), 9Cr CNA (cast nanostructured alloy), and two Fe-12Cr-5Al ODS (oxide-dispersion strengthened) alloys (Y-Zr FeCrAl and Y-Hf FeCrAl) were irradiated. Advanced characterization was used with the intent of analyzing the changes to the microstructure driven by the irradiation, particularly to determine how helium bubbles are dispersed in the four different materials. Because no intense 14 MeV neutron sources are available, these accelerator-based tests are the most effective way to screen candidate alloys for helium mitigation potential.

Experimental Procedure

The alloys were mechanically polished to colloidal silica and irradiated at 650°C to provide ~800 appm He, followed by 2.75 MeV Fe ion irradiation to produce a midrange dose of ~50 dpa at 650°C; Figure 1.

Samples for electron microscopy were prepared by FIB (focused ion beam) milling from the irradiated areas. S/TEM (Scanning / transmission electron microscopy) was performed using FEI Tecnai T20 or FEI Talos F200X instruments at ORNL. In particular, STEM imaging using conventional and Fresnel-STEM [1] modes were used to image precipitates and helium bubbles simultaneously. X-ray spectrum images (SIs) were taken using the F200X instrument's high-efficiency, 4-detector system. Some of the SIs were analyzed using the Sandia National Laboratory AXSIA computer code [2] to perform multivariate statistical analysis [3].

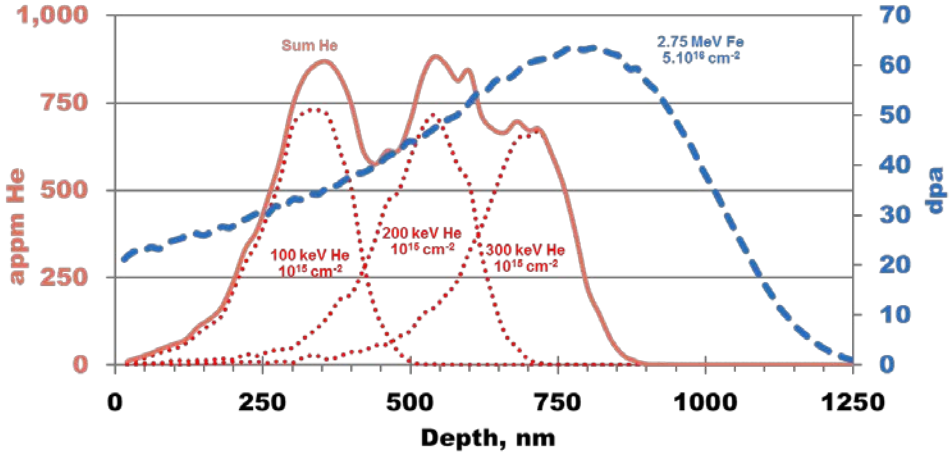

Figure 1. SRIM-software calculations of the expected He and dpa profiles for the irradiations. The appm/dpa ratio is ~10-20, reasonably representative for a fusion spectrum on a ferritic steel.

Results

Analysis of the samples is presently underway; however, preliminary scoping results, especially indicating the capabilities of the new F200X microscope at ORNL to explore helium mitigation, will be presented here.

The 9YWTV NFA material, under the present sequential 650°C irradiations, appears to have best sequestered the helium in terms of uniform matrix dispersal, compared to the other three materials (CNA, Y-Zr FeCrAl, Y-Hf FeCrAl). Experiments are ongoing and this preliminary observation may be revised. The 9YWTV shows the smallest helium bubbles, and a large fraction of the bubbles are captured in the grain interiors, away from the grain boundaries.

For instance, Fresnel-contrast BF STEM and HAADF STEM at ~700 nm depth (~800 ppm He, ~50 dpa) shows a high density of very fine bright/dark features in Fresnel imaging, presumed to be bubbles, along with bands of dark features in HAADF, presumably nanoclusters (Figure 2). An X-ray mapping experiment was performed in the F200X instrument, which provided a high statistical confidence for mapping the locations of the nanoclusters (Figure 3).

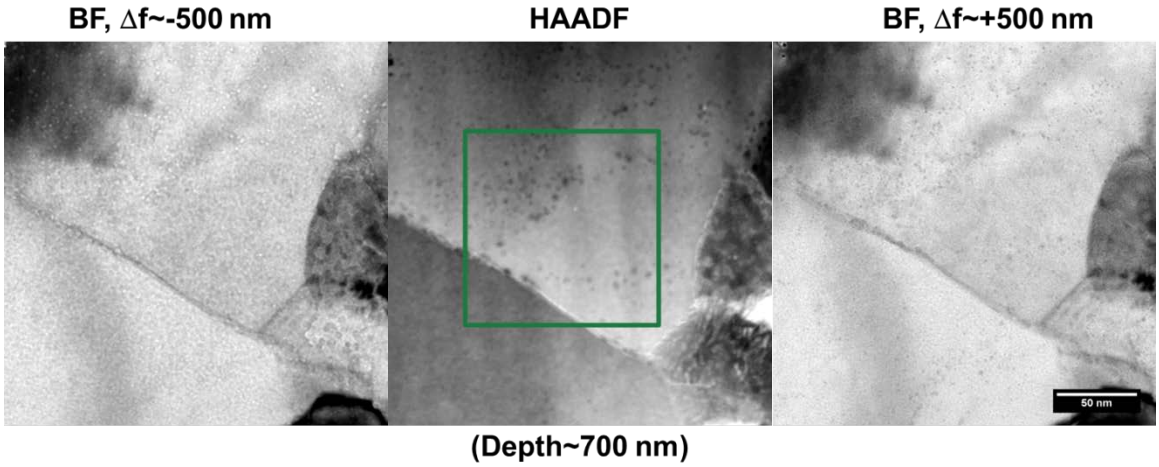

Figure 2. 9YWTV, sequential He + Fe irradiation, 650°C. Fresnel BF-STEM and HAADF-STEM images showing void-like contrast (presumably He bubbles) along with grain boundary and precipitates.

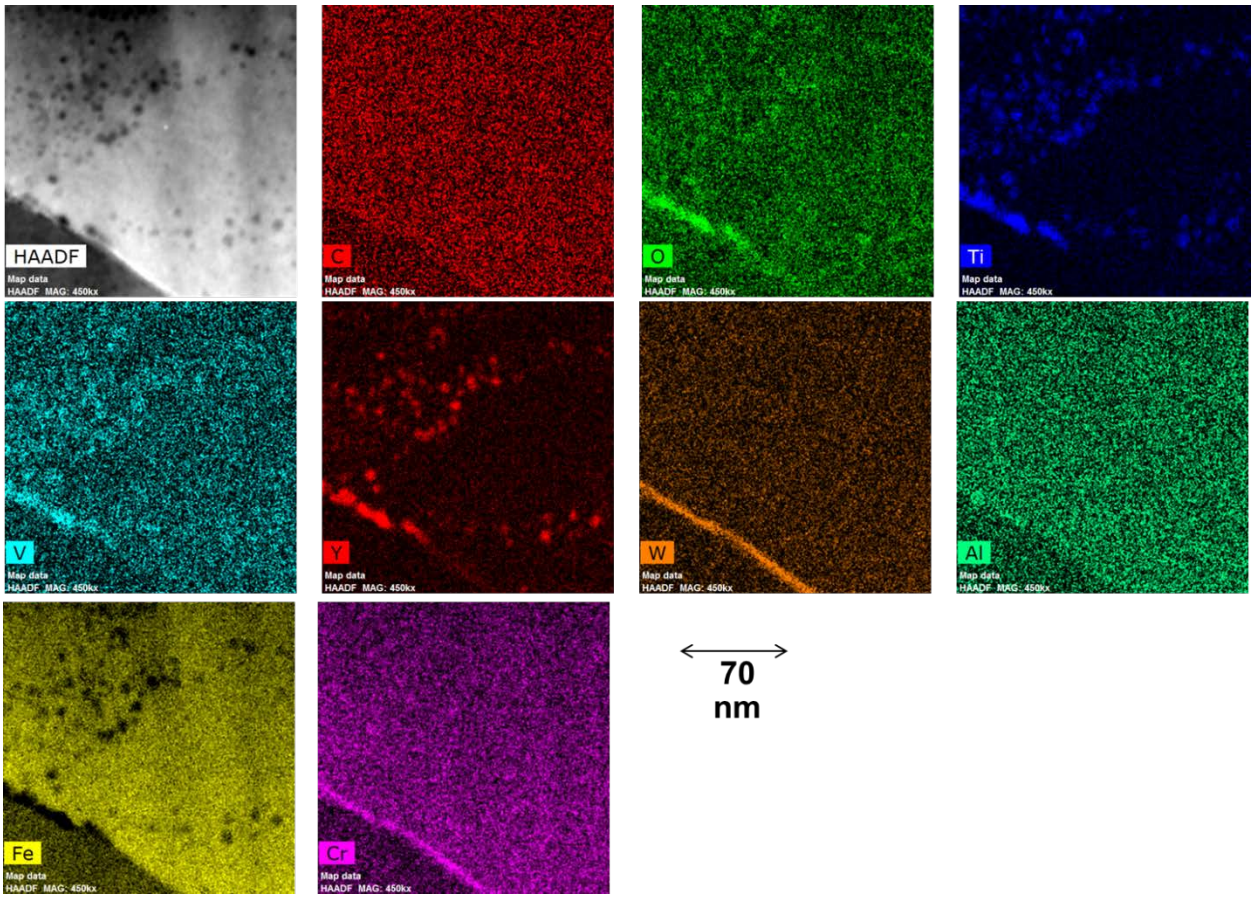

Figure 3. Same area as Figure 2, X-ray mapping. Note Cr-W on grain boundary and Y-Ti-O in nanoclusters.

The distribution of the nanoclusters can be more precisely defined by applying MVSA to the spectrum image dataset from which the X-ray maps (Figure 3 above) were extracted. MVSA analysis (Figure 4) decomposed the data into three underlying components, indicating matrix (Fe-Cr), grain boundary enrichment (Cr-W) and nanoclusters (Ti-Y-O). Most importantly, the visibility (contrast) of the nanoclusters is improved (Figure 3, right panel) compared to their visibility in the X-ray maps (Figure 2) due to the statistical ensemble averaging of the data.

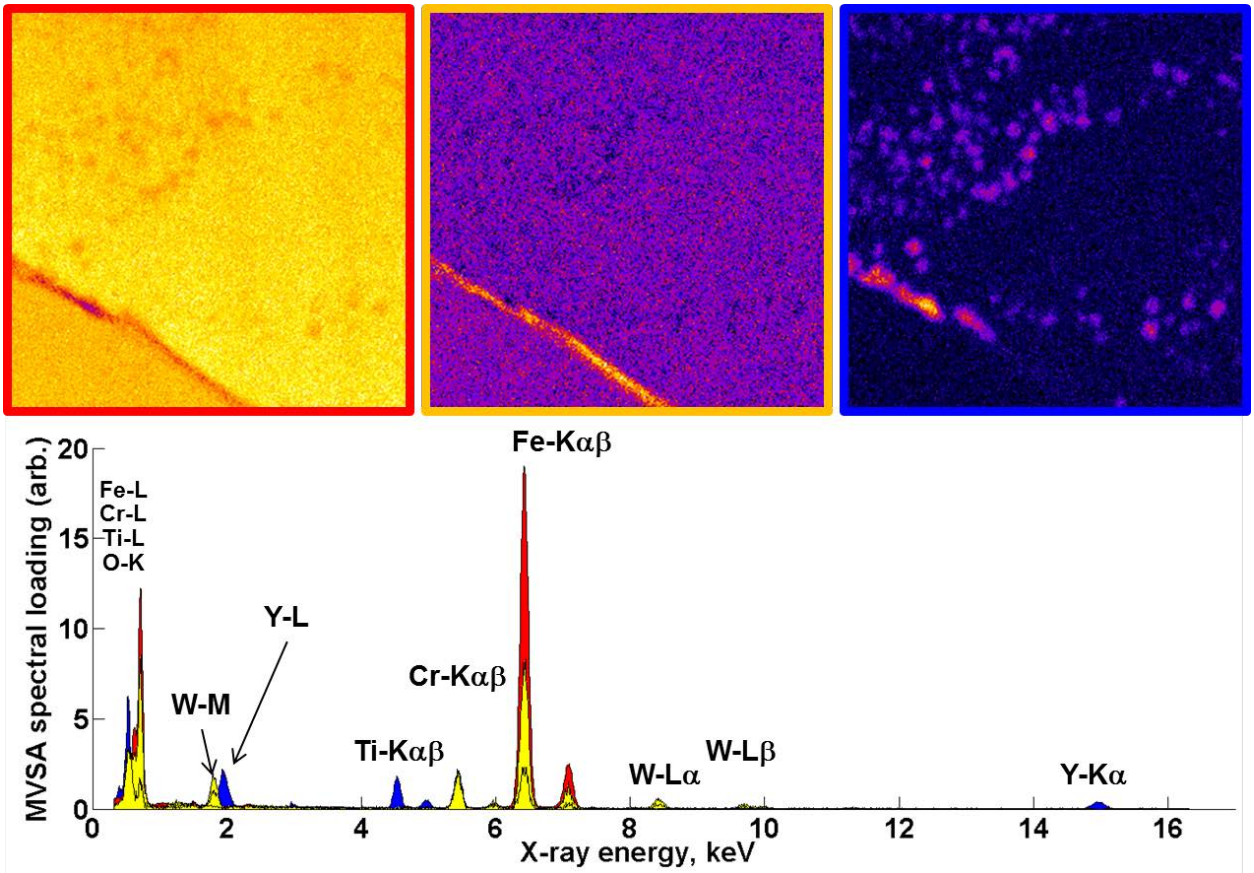

Figure 4. Multivariate statistical analysis of the X-ray mapping data in Figure 3. Note improved visibility of the nanoclusters (blue spectrum, blue-bordered image) compared to the X-ray maps (Figure 3).

Combining the MVSA component image with the Fresnel-contrast STEM image (Figure 5) indicates that the bubble-like contrast and the nanoclusters appear to be closely associated; there appear to be slightly more bubbles than nanoclusters, however. This implies that the nanoclusters are sequestering the helium effectively, although further confirming experiments are needed.

The CNA alloy appears to show more helium bubbles at dislocations, grain boundaries and lath boundaries, and larger bubbles, than the 9YWTV alloy (Figure 6). X-ray analysis indicates significant Ti content at or near the same locations as the Fresnel contrast of the bubbles. X-ray mapping (Figure 7) and MVSA (Figure 8) show the same result.

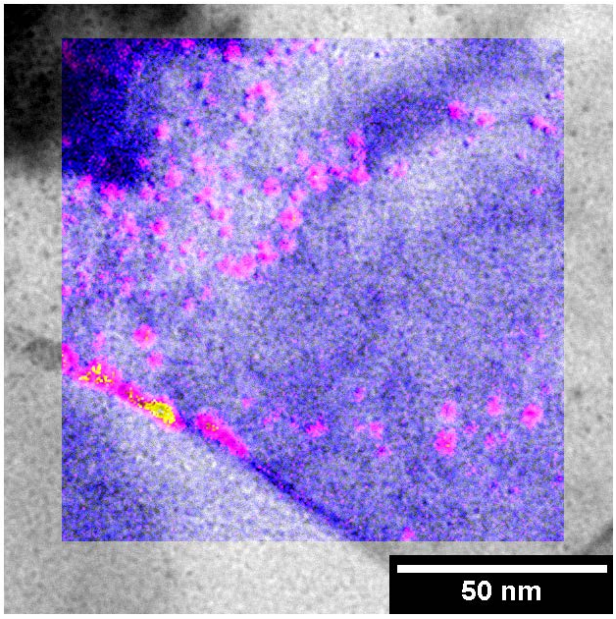

Figure 5. MVSA nanocluster map overlaid onto the Fresnel-STEM image. It appears that the presumed bubble contrast is mostly associated with the nanocluster features.

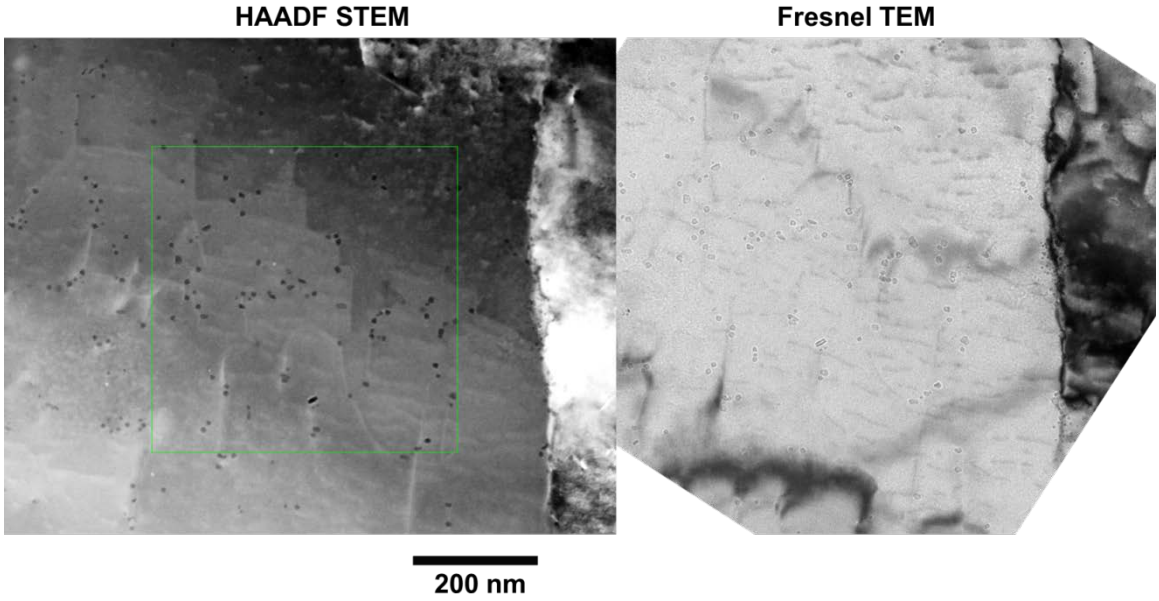

Figure 6. HAADF-STEM image showing low-atomic-number regions (bubbles or precipitates), and Fresnel TEM image, showing void contrast.

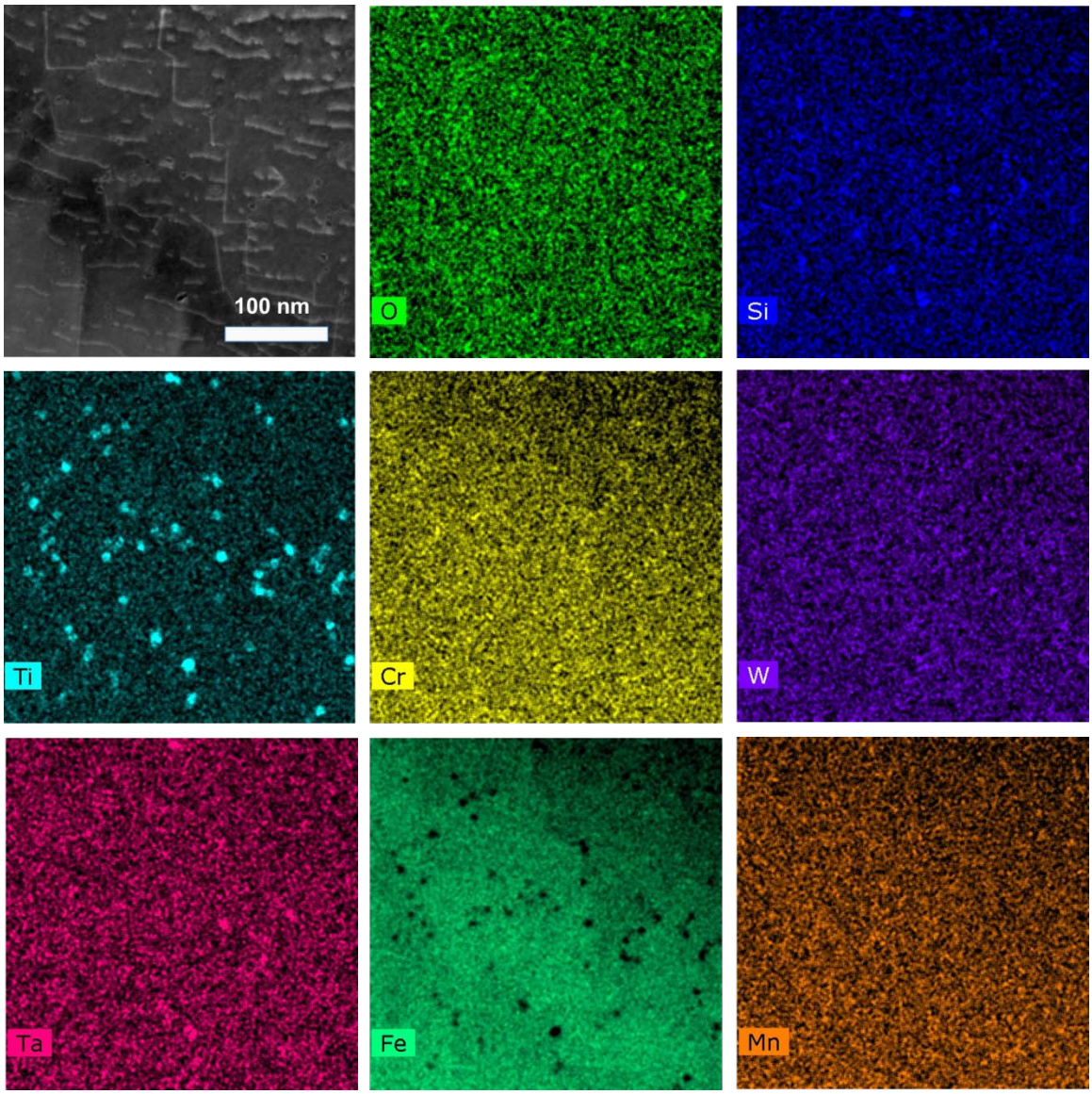

Figure 7. HAADF-STEM image and X-ray maps from the area of Figure 6. Note the Ti-rich regions that appear associated with cavity-like contrast.

Although further microscopy, and perhaps atom probe tomography, is needed, it is possible that the Ti-rich features in Figures 7 and 8 may be helium bubbles, showing Ti-enrichment to the region of the bubbles, or perhaps to their surfaces.

Further work on unirradiated regions of the CNA alloy (to compare to Figures 6-8), and characterization of the bubbles in the He+Fe irradiated FeCrAl samples, is presently underway. The dual-ion-beam irradiated samples will also be examined for comparison to these sequentially-irradiated samples.

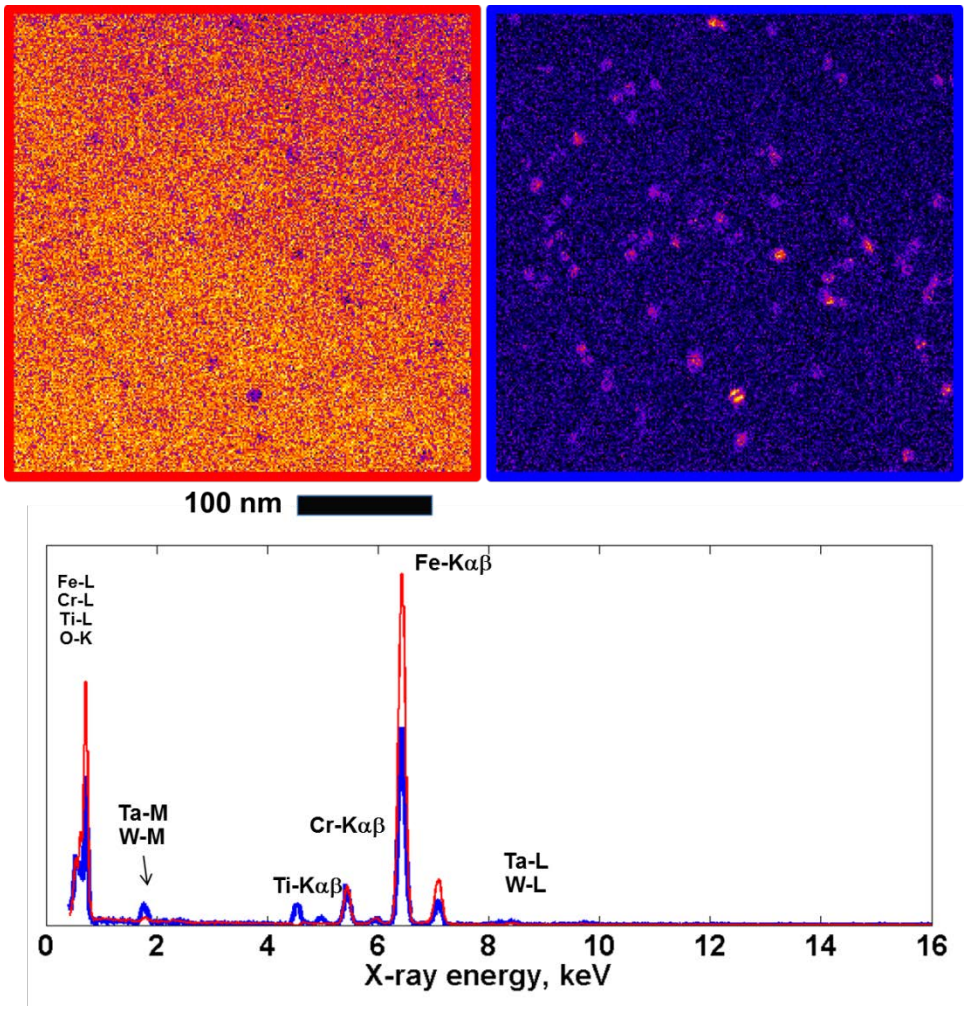

Figure 8. MVSA component maps and spectra of the X-ray data presented in Figure 7. Strong Ti contrast is associated with the features seen in the X-ray maps.

Acknowledgements

9YWTV material provided by Dr. T. S. Byun. Talos F200X STEM provided by the Department of Energy, Office of Nuclear Energy, Fuel Cycle R&D Program and the Nuclear Science User Facilities.

References

[1] C.M. Parish, M.K. Miller, Aberration-Corrected X-Ray Spectrum Imaging and Fresnel Contrast to Differentiate Nanoclusters and Cavities in Helium-Irradiated Alloy 14YWT, Microscopy and Microanalysis, 20 (2014) 613-626.

[2] P.G. Kotula, M.R. Keenan, J.R. Michael, Automated analysis of SEM X-ray spectral images: a powerful new microanalysis tool, Microscopy and Microanalysis, 9 (2003) 1-17.

[3] C.M. Parish, Multivariate Statistics Applications in Scanning Transmission Electron Microscopy X-Ray Spectrum Imaging, in: P.W. Hawkes (Ed.) Advances in Imaging and Electron Physics, Vol 168, 2011, pp. 249-295.